Plasmon production by the decay of hollow Ne atoms near an Al surface

N. Stolterfoht, D. Niemann, V. Hoffmann, M. Rösler, and R. A. Baragiola*
Hahn-Meitner-Institut Berlin GmbH, Bereich Festkörperphysik, D-14109 Berlin, Germany
(Received 1 November 1999; published 17 April 2000)

Measurements of low-energy electrons emitted by 4.5-keV Ne^{q+}-ion impact on an Al surface are discussed for incident charge states $q=1-6$. Spectral structures found near 11 eV are attributed to the decay of bulk plasmons. A method is given to determine absolute values for the experimental electron yield from the plasmon decay. Absolute plasmon yields are studied as a function of the incidence angle of the projectile and the observation angle of the electron. A cosinelike angular distribution is found for the ejected electrons indicating that the plasmons decay well below the surface. The experimental data are compared with model calculations providing information about the plasmon production mechanisms.

PACS number(s): 79.20.Rf, 34.50.Dy, 71.45.Gm, 73.20.Mf

I. INTRODUCTION

Valence electrons in metals can take part in quantized collective oscillations known as plasmons. The excitation of plasmons by charged particles can be described within the framework of the free-electron-gas approximation [1,2] in conjunction with the random-phase approximation (RPA) [2,3]. For nearly-free-electron metals (e.g., Al) plasmons decay predominantly by transferring energy into a single valence electron in an interband transition [4,5]. Hence, electrons of characteristic energies are ejected from the metal providing a signature for plasmons that can experimentally be studied by means of electron spectroscopy [6–8]. Most previous experiments with ion impact [7–9] have been performed using fast projectiles that create plasmons via direct Coulomb excitation. However, this mechanism is constrained by momentum and energy conservation and thus requires a threshold velocity, corresponding to a minimum energy of about 33 eV for electron impact and 40 keV/u for heavy particles incident on Al [10].

Recently, evidence for plasmon excitation has been provided from electron emission spectra produced by ions with energies below a few keV [11–15]. In those studies, it was commonly accepted that mechanisms different from direct Coulomb excitation are important, especially for heavy ions. However, different ideas have been put forward to interpret the creation of plasmons by slow ions. Various groups [11,12,16–18] have considered plasmon-assisted capture processes where the transfer of potential energy from the projectile produces a plasmon. On the other hand, kinetic energy effects have been taken into consideration for proton impact [13,14]. Recent theoretical calculations have shown that high-energy electrons liberated in binary collisions with the projectiles may produce plasmons in secondary collisions, even at subthreshold ion velocities [13].

Here, the attention is focused on slow heavy ions incident on a surface with a high charge state [12]. The characteristic feature of a highly charged ion is its large potential energy. Hence, plasmon creation may be enhanced when potential energy effects become significant. The large potential energy of highly-charged ions has attracted much interest in studies of ion-solid interactions (see [19] and references therein). Above the surface, highly-charged ions strongly attract several electrons that are resonantly captured into high Rydberg states whereas inner shells remain empty. Thus, the projectiles evolve into hollow atoms whose formation and decay imply various novel processes.

When a hollow atom enters into the solid the remaining Rydberg electrons are removed (peeled off) or enter into the solid to participate in the formation of a strong screening cloud of conduction-band electrons referred to as the *C* cloud [20]. The *C* cloud leaves inner shells empty so that a compact hollow atom is formed below the surface. When the hollow atom moves within the solid, it transfers its potential energy via Auger transitions and collisional charge transfer [21,22]. Moreover, the interaction of the hollow atom with the solid leads to the production of plasmons by potential-energy effects [12].

In this work we study plasmon creation by the impact of 4.5-keV Ne^{q+} on Al with charge states from $q=1-6$. The electron spectra indicate structures near 11 eV associated with the decay of bulk plasmons which remain significant for charge states as large as $q=5$. Our previous experiments for an observation angle of 75° [12] were extended with measurements for which both the incidence angle of the projectile and the observation angle of the electron were varied. A spectral analysis is introduced to obtain absolute yields for plasmon production. The experimental results are compared to model calculations of the cascading decay of hollow atoms, which involve potential-energy transfers including the selective creation of bulk plasmons at a few atomic layers below the surface.

II. EXPERIMENTAL METHOD

The measurements were carried out at the 14.5-GHz electron cyclotron resonance (ECR) source at the Ionenstrahl-Labor (ISL) in Berlin using an ultrahigh vacuum chamber equipped with a rotatable electron spectrometer [23,24]. The

*Permanent Address: Laboratory for Atomic and Surface Physics, University of Virginia, Engineering Physics, Charlottesville, VA 22901.

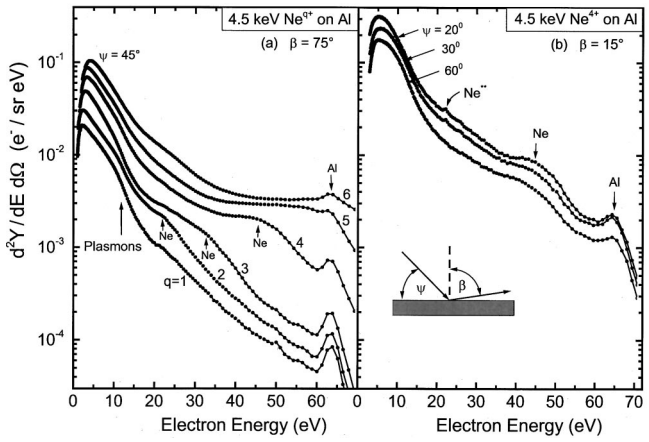

FIG. 1. Double differential emission yields $d^2Y/dEd\Omega$ for electrons produced by a 4.5-keV Ne^{q+} incident on an Al surface. In (a) the spectra are obtained for the projectile charge states $q=1-6$ [12]. The incident angle is $\psi=45°$ relative to the surface plane and the observation angle is $\beta=75°$ relative to the surface normal. In (b) Ne^{4+} spectra are given for the observation angle $\beta=15°$ and different incident angles $\psi=20°,30°$, and 60°. The maxima labeled Al and Ne are due to *L*-shell Auger electrons from the Al target and the Ne projectile, respectively.

experimental method has been presented before [12,25] so that only a brief description will be given. Beams of 4.5-keV Ne^{q+} $(q=1-6)$ ions were collimated to a diameter of about 1 mm and directed onto a clean Al target. The pressure in the chamber was a few 10^{-10} mbar. The emission of electrons from the target was measured using an electrostatic parallel-plate spectrometer [26]. The spectrometer efficiency and the ion current were determined [23] so that absolute values for electron emission yield could be measured. The experimental setup was optimized to accurately measure low-energy electrons [27]. Our experience shows that the spectrometer is capable of measuring reliable electron yields for energies as low as 2–4 eV.

Figure 1(a) shows experimental results for the double differential electron emission yield $N(E)=d^2Y/d\Omega\, dE$ at an angle of incidence of $\psi=45°$ and an observation angle of $\beta=75°$ relative to the surface normal [12]. The electron spectrum for each charge state exhibits a maximum at low energies. For kinetic electron emission, a maximum is expected at about 2 eV [28–30] and, indeed, observed for low projectile charge states (e.g., Ne^+). The kinetic electron emission peak exhibits a shift in energy with increasing charge state, which calls for further studies. Moreover, in Fig. 1(a), one can see a significant increase of the electron yield with increasing charge state. This is due to the increase of potential electron emission [31] which is found to be roughly proportional to the corresponding potential energy.

Electron emission by highly charged ions is primarily caused by dielectronic processes above and below the surface [27]. Above the surface, autoionizing transitions among high Rydberg states give rise to electron energies as low as a few eV, whereas Auger transitions in inner shells take place primarily below the surface, especially for highly charged projectiles. The emission of *L*-shell Auger electrons from

TABLE I. Electronic transition energy from the bottom of the conduction band of Al to the $2p$ level of a hollow Ne atom which contains a number of $2p$ vacancies. The results are based on total energies evaluated using the density-functional theory [22]. Note that the transition energies may be reduced by electron promotion effects when the hollow Ne atom collides with an Al lattice atom [21].

Number of $2p$ vacancies	1	2	3	4	5	6
Transition energy (eV)	12.8	23.6	33.4	45.6	56.7	68.8

Ne^{q+} projectiles for $q=2,3$, and 4 are seen with centroid energies near 22, 34, and 46 eV, respectively. The increase of the *L*-shell Auger electron energy with charge are given in Table I, indicating that the energy liberated by electron transitions into the Ne *L* shell becomes larger as the number of Ne $2p$ vacancies increases. Apart from the projectile Auger electrons, the spectrum in Fig. 1(a) shows distinct peaks near 63 eV due to the Auger decay of Al $2p$ vacancies [7] excited in binary collisions with a hollow Ne projectile [21] or in Al-Al collisions involving fast recoils [32]. A significant fraction of these electrons originates from sputtered Al decaying outside the solid.

Figure 1(b) shows electron spectra observed at an emission angle of $\beta=15°$ for different incidence angles of the Ne^{4+} projectiles ($\psi=20°,30°$, and 60°). The $\beta=15°$ spectra in Fig. 1(b) are larger in intensity than the corresponding Ne^{4+} spectrum observed at $\beta=75°$ in Fig. 1(a) due to the $\cos\beta$ dependence of the electron emission (see below). Also, the spectral intensity increases with decreasing incidence angle ψ. This finding is likely due to an increase of the interaction time of the hollow atom near the surface. Apart from the Ne and Al *L*-shell Auger maxima mentioned above, one finds a distinct peak at 22 eV, labeled Ne**, which can be attributed to above-surface emission of Auger electrons from Ne with two vacancies in the *L* shell [33]. This shows that a noticeable fraction of the Ne^{4+} projectiles captures two electrons into the *L* shell and undergoes an *L*-shell–Auger-electron transition in front of the surface. As expected this above-surface capture is enhanced with decreasing incidence angle of the projectile as seen in Fig. 1(b).

The structures due to bulk plasmon decay are expected near 11 eV (Fig. 1). To enhance the visibility of the plasmon structures, which are superimposed on an intense background from other processes, it is common practice to differentiate the measured electron intensities $N(E)$ [4]. Results for $q=1,2$, and 4 are presented in Figs. 2(a)–2(c) [12]. Note that the derivative dN/dE increases with charge state similarly as the original spectra in Fig. 1. The derivative dN/dE for $q=1$ clearly shows a structure near 11 eV which is commonly attributed to bulk plasmons. This structure is enhanced for $q=2$ but becomes less pronounced in comparison with the background as the charge state further increases to $q=4$.

As in previous work [11,12,17] we consider excitation by potential-energy transfer as a primary mechanism for plasmon production by slow heavy ions. This mechanism involves the capture of a valence electron into the *L* shell of the

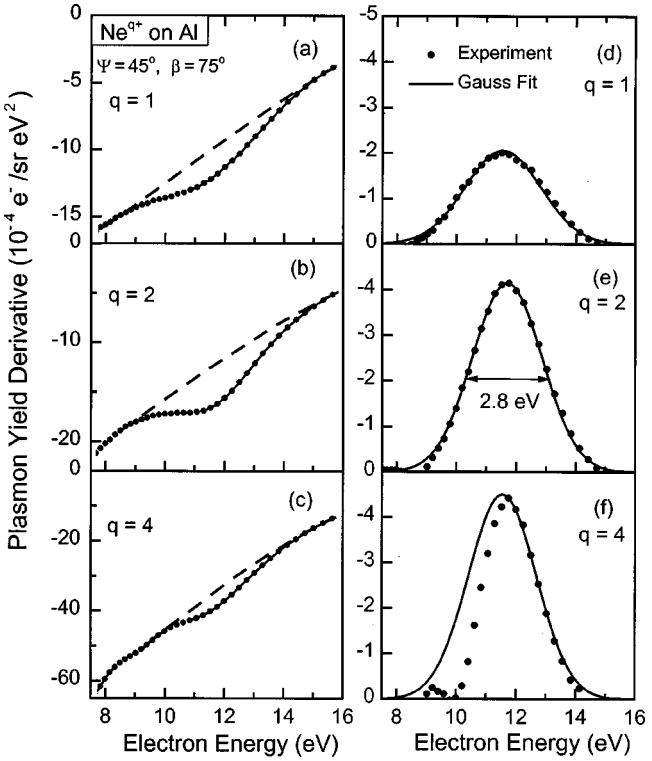

FIG. 2. Derivative dN/dE of the double differential emission yields given in Fig. 1. The results in (a), (b), and (c) refer to 4.5-keV Ne^{q+} impact where $q=1,2$, and 4, respectively. In (d), (e), and (f) the corresponding data are shown after subtraction of the continuous background. The experimental data are fit with Gaussian functions using a constant centroid energy and width.

Ne projectile, which provides the energy for plasmon creation [16]. However, other mechanisms for plasmon creation may be considered. Note first that Ne orbitals higher than the $2p$ shell cannot participate in the bulk-plasmon creation, since those orbitals are not bound inside the solid [22]. However, energetic electrons produced directly in collisions as well as Auger electrons may excite plasmons when traveling through the solid [13].

III. SPECTRAL ANALYSIS AND ANGULAR DISTRIBUTIONS

To obtain more information about the mechanisms for plasmon production, absolute values for the corresponding electron emission yield were extracted from the electron spectra. The principles of the procedure are shown in Fig. 3. The energy ε_p liberated by the decaying plasmon is determined by the Lorentzian function $\mathcal{L}(\varepsilon_p, E_p, \Gamma_p)$ involving the plasmon energy $E_p=\hbar\omega_p$ and decay width Γ_p. In Fig. 3(a) the Lorentzian, represented by the curve labeled *Initial Distribution*, is normalized to the unit area. The energy distribution of the electrons excited from the conduction band is obtained as a convoluting over the normalized density of states $\mathcal{D}(E)=N\sqrt{E}$ for $E\leqslant E_F$, see Fig. 3(b). With the normalization factor $N=E_F^{-1/2}$ the integral of the $\mathcal{D}(E)$ function is obtained as $2E_F/3$. The convolution is performed by the integration

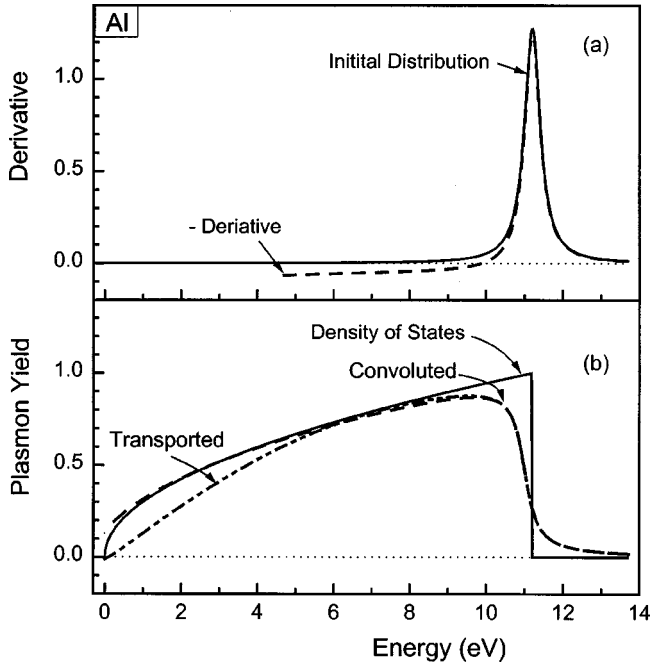

FIG. 3. Method to determine absolute electron yields originating from plasmon decay. In (a) a Lorentzian function is shown with a width of $\Gamma_p=0.5$ eV representing the *Initial Distribution* of the energy liberated by the plasmon decay (shifted to the Fermi energy $E_F=11.2$ eV of Al). In (b) the *Density of States* in the Al conduction band normalized to unity at E_F is compared with the *Convoluted* curve obtained by convoluting the density of states with the initial energy distribution. The curve labeled *Derivative* represents the (negative) derivative of the convoluted curve. Also, (b) shows a curve labeled *Transported* which includes electron transport effects by the solid, such as attenuation and refraction.

$$F(\varepsilon)=\int_0^{E_F}\mathcal{L}(\varepsilon+U-E,E_p,\Gamma_p)\mathcal{D}(E)dE, \qquad (1)$$

where U is the potential step at the surface (15.5 eV for Al) and ε is the energy of the plasmon-decay electron outside the solid. The result of the convolution is represented by the data labeled *Convoluted* in Fig. 3(b) whose integral remains equal to $2E_F/3$. [The convoluted curve was shifted in energy so that a direct comparison is possible with the $\mathcal{D}(E)$ curve.]

The crucial point of the present method is that the derivative of the $F(\varepsilon)$ curve, also given in Fig. 3(a), reproduces closely the initial energy distribution of the plasmon. Thus, the intensity of the plasmon-decay electrons is obtained from the integral of the *Derivative* curve multiplied by $2E_F/3$. It should be noted that this factor is independent of the shape of the initial plasmon energy distribution. To account for the transport of the electrons, attenuation and refraction effects have to be considered; this leads to the curve labeled *Transported* in Fig. 3(b). When the *Transported* curve is normalized to the *Convoluted* curve near E_F, the transport effects are found to be small (the factor $2E_F/3$ is reduced by $\sim 20\%$). It is noted that the density of states of the conduction band is distorted by the presence of a charged particle. For low charge states, such distortion has been found to be

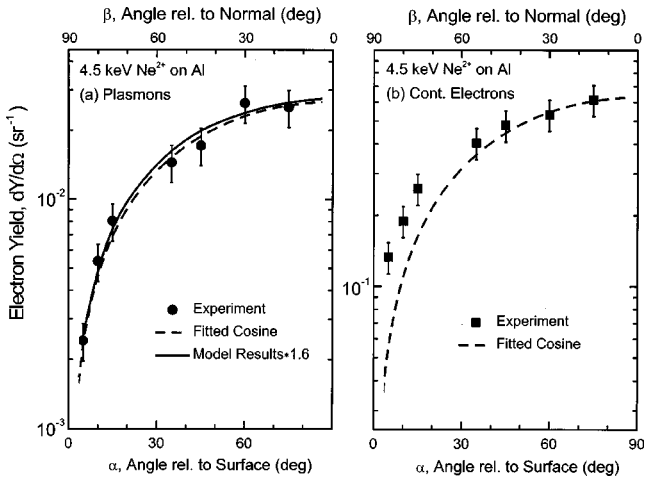

FIG. 4. Angular distribution of electron yields obtained by 4.5-keV Ne^{2+} impact on Al. The results refer to electrons due to plasmon decay (a) and the total amount of continuum electrons (b). Both the angles β relative to the surface normal (upper scale) and α relative to the surface plane (lower scale) are shown. The experimental results (points) are compared with cosine functions normalized near the angle $\alpha=90°$ (dashed curve) and with model calculations based on Eq. (4) (solid curve). Note that the model results are multiplied by 1.6.

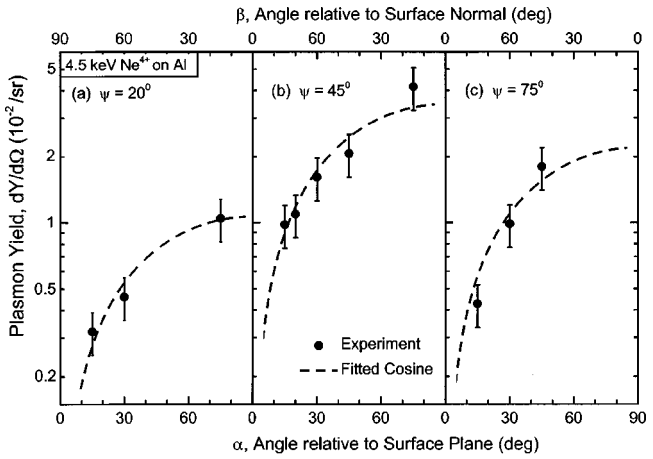

FIG. 5. Angular distributions of electrons from plasmon decay obtained by 4.5-keV Ne^{4+} impact on Al. Both the angles β relative to the surface normal (upper scale) and α relative to the surface plane (lower scale) are shown. In (a), (b), and (c) data are given for the incidence angles $\psi=20°,45°$, and 75°, respectively. The experimental results (points) are compared with cosine functions normalized to fit the experimental data (dashed curves).

small [13]. These effects, however, may increase with increasing projectile charge [22,47].

Figure 2 shows examples for the analysis of the experimental derivative curves. After background subtraction these curves were fit by Gaussian functions. From Fig. 2(e) it is seen that the width of the derivative curve is relatively large (2.8 eV) showing that broadening effects have altered the peak profile from a Lorentzian to a Gaussian (Fig. 2). This may partially be due to the transfer of finite plasmon momenta which causes a variation of the plasmon energy E_p [4]. Fortunately, as noted above, the deduction of the absolute plasmon yield is independent of the shape of the derivative curve. It should be realized that the background subtraction involves uncertainties which influence primarily the left-hand side of the *Derivative* curve. Therefore, the right-hand side of the derivative curve was preferentially used for the fit in Fig. 2(f).

It should be recalled that the data in Fig. 2 refer to a single observation angle ($\beta=75°$). For Ne^{2+} and Ne^{4+} impact, electron emission yields have also been measured for various observation angles of the electrons. The knowledge of the angular dependence is crucial for different reasons. First, it is well known that electrons originating in the bulk of the solid exhibit a cosinelike angular dependence [34]. On the other hand, electrons originating from shallow surface layers are expected to exhibit a more isotropic emission [23,24]. Hence, the observed angular dependence of the plasmon-decay electrons provides information about the depth of the plasmon production. Furthermore, information about the angular dependence is required when total yields of electrons ejected into the hemisphere above the surface are evaluated.

For the angular dependent emission yields we performed an analysis of the spectral derivatives similar to that in Fig. 2. The results for Ne^{2+} projectiles are given in Fig. 4(a) which refer to the absolute values of the plasmon yields differential in angle [25]. The lower and upper x scales show the electron observation angles α and β measured relative to the surface plane and surface normal, respectively. The experimental results are seen to follow closely a normalized cosine distribution, providing evidence that the plasmons are produced (and decay) well inside the solid. Plasmon excitation will be analyzed in more detail when the model calculations are discussed below. To demonstrate that the cosine distribution is not always found, Fig. 4(b) shows the angular distribution of electrons integrated over all energies. The data exhibit an angular dependence that is weaker than the cosine dependence. This may indicate that some of the low-energy electrons are created outside the solid. In Fig. 1 the spectra are governed by low-energy electrons that may be produced by autoionizing transitions in higher Rydberg states formed above the surface [25].

Figure 5 gives the results for incident Ne^{4+} obtained using the same fit procedure as before. The experimental data are seen to closely follow normalized cosine functions, providing again evidence that the plasmons are produced well inside the solid. For Ne^{4+} projectiles we studied the plasmon yield with respect to a varying incidence angle of the projectile. In Figs. 5(a)–5(c) results are shown for incidence angles of $\psi=20°,45°$, and 75°, respectively. It is seen that the plasmon yields are relatively small at the gracing incidence angle of 20°. The data are largest at 45° whereas a decrease is observed for 75°. These findings may indicate that at small angles the incident hollow atoms are partially deexcited in front of the surface by Auger neutralization or by production of surface plasmons. In this case, the projectiles lose their ability to excite bulk plasmons. At large angles the ions travel deeply into the solid so that both secondary electrons and electrons from the plasmon decay are attenuated. Thus,

an optimum value for plasmon excitation may be expected at intermediate incidence angles near 45°.

IV. MODEL CALCULATIONS

In the past, for the cascading decay of hollow atoms, various models have been developed that can be divided into two groups: (i) models treating the mean number of electrons in a given shell [35–38] and (ii) models treating the occupation number of individual configurations [21,39–41]. For the latter case, we shall present an analytic evaluation describing the first step of the filling sequence of a hollow atom. This formalism exhibits the various parameters relevant for the creation of plasmons by slow ions. For the yields of Ne *L*-shell Auger electrons, we shall consider an extension of the model referring to a combination of the mean-charge and configuration methods [42].

When a highly charged ion such as Ne^{q+} enters into a solid, the screening cloud *C* of valence-band electrons is rapidly formed around the ion (in $\sim 10^{-16}$ sec). Then, *LCC* Auger transitions take place with the rate Γ_{LCC} reducing the charge state *q* in the *L* shell. Similar effects lead to plasmon creation with the rate Γ_{pl}. Since the production of plasmons and *L*-shell Auger electrons are competing processes we use the branching ratios $b_i = \Gamma_i / \Gamma_L$ where $\Gamma_L = \Gamma_{LCC} + \Gamma_{pl}$ is the *L*-shell filling rate and the label *i* stands either for plasmon creation or *L*-shell Auger transitions.

Besides plasmon and *L*-shell Auger-electron production, collisional charge transfer with the rate Γ_{col} may fill the Ne *L* shell [21]. Hence, the occupation number N_q of the initial configuration, decaying with the sum rate $\Gamma_s = \Gamma_{LCC} + \Gamma_{pl} + \Gamma_{col}$, is obtained as $N_q = f_o e^{-\Gamma_s t}$, where f_o is the survival fraction of the Ne^{q+} ions in front of the surface. Time *t* transforms to depth $z = v_z t$ by means of the vertical ion velocity v_z and rates are defined in terms of unit depth, i.e., $\tilde{\Gamma}_L = \Gamma_L / v_z$ and $\tilde{\Gamma}_s = \Gamma_s / v_z$. Assuming isotropic ejection of electrons from plasmon decay and from *L*-shell Auger transitions one obtains for the electron yield per unit solid angle and depth

$$\frac{dY_i'}{d\Omega' dz} = \frac{f_o}{4\pi} b_i \tilde{\Gamma}_L e^{-\tilde{\Gamma}_s z}, \tag{2}$$

where primed quantities such as the solid angle $d\Omega'$ refer to inside the solid. Finally, electron transport effects are taken into account to obtain the emission yield outside the solid

$$\frac{dY_i}{d\Omega\, dz} = \frac{f_o}{4\pi} e^{-z/\lambda_L \cos\beta'} b_i \tilde{\Gamma}_L \frac{\varepsilon \cos\beta}{(\varepsilon + U)\cos\beta'} e^{-\tilde{\Gamma}_s z}. \tag{3}$$

It is recalled that *U* is the potential step at the surface and ε is the electron energy outside the solid. Due to refraction effects the emission angle β' inside the solid is altered to β outside the solid relative to the surface normal. The transport of the electrons is approximately taken into account by exponential attenuation involving the attenuation length λ_L.

Equation (3) can readily be integrated over the emission depth z

TABLE II. Branching ratios for plasmon production for different numbers of vacancies in the *L* shell of Ne (from the work by Díez Muiño [44]).

Number of $2p$ vacancies	1	2	3	4
Branching ratio	0.53	0.35	0.05	<0.01

$$\frac{dY_i}{d\Omega} = \frac{f_o}{4\pi} \frac{\lambda_L}{1 + \lambda_L \tilde{\Gamma}_s \cos\beta'} b_i \tilde{\Gamma}_L \frac{\varepsilon}{\varepsilon + U} \cos\beta. \tag{4}$$

It shows that the angular dependence may vary from an isotropic ($\lambda_L \tilde{\Gamma}_s \gg 1$ and $\beta' = \beta$) to a cosine dependence ($\lambda_L \tilde{\Gamma}_s \ll 1$). The latter case refers to a significant attenuation within the emission depth of the electrons.

It is recalled that Eqs. (3) and (4) are limited to describing only the first step of the decay sequence for hollow atoms. More information about the further steps of the decay sequence may be obtained from Ref. [21], where also most of the model parameters are given. In particular, for the *L*-shell occupation number $l = 0$ we adopted the Ne *L*-shell filling rate $\Gamma_L = 5 \times 10^{-3}$ a.u. [21]. For $l = 7$ the rate $\Gamma_L = 2 \times 10^{-2}$ a.u. was chosen [43] and a linear interpolation was performed to obtain the rates for the intermediate values of *l*. The branching ratios b_{pl} for plasmon production by Ne^{q+} have been calculated by Díez Muiño [44]. The results are given in Table II indicating that plasmon production is significant for Ne^{q+} with charge states $q = 1$ and 2, whereas it becomes negligible for higher charge states. To determine the attenuation length λ_L no unique method is available. For λ_L we used a value of 14 a.u. for plasmon-decay electrons, taken from an analysis using a Monte Carlo calculation [45].

An example for model calculations are given in Fig. 4(a) which shows theoretical results for electron emission by plasmon excitation through Ne^{2+} impact on Al. The model calculations were performed with $f_o = 1$ using Eq. (4) for the first step ($q = 2$) of the decay sequence of the hollow Ne. Similarly, the contribution of the second step ($q = 1$) was evaluated as in Ref. [21]. The contributions from the two steps are found to be of similar importance showing that Eq. (4) is not sufficient for the present case. The model calculations are found to follow closely the cosine function. However, the theoretical results are about 60% smaller than the experimental data (note that the model results are multiplied by 1.6).

To obtain information about the location of the plasmon production, we performed calculations of the depth-dependent electron yield. The results are plotted in Fig. 6 showing the electron yield for the angles of 0° and 75° as a function of the emission depth. For 0° results are also given without attenuation, indicating that attenuation effects are important in the present case. The first step ($q = 2$) of the decay sequence follows an exponential function as predicted by Eq. (3). The contribution of the second step ($q = 1$) is found to be significant. As mentioned above, the two steps contribute by about equal amounts.

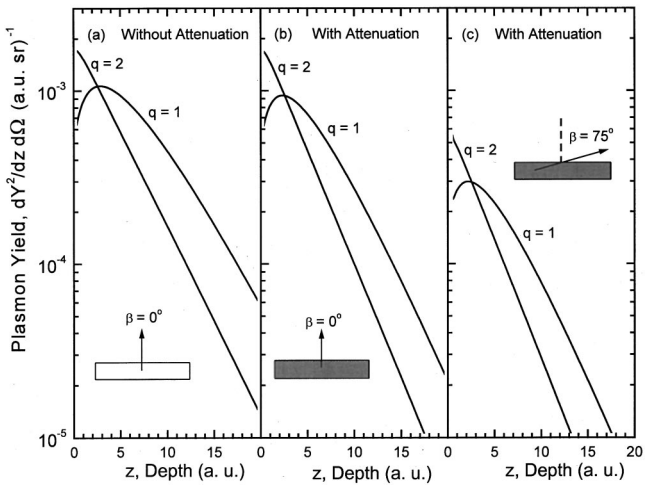

FIG. 6. Electron emission yield $d^2Y/dz\,d\Omega$ for plasmon decay by impact of 4.5-keV Ne^{2+} on Al as a function of the depth z. In (a) results are shown without attenuation but with refraction for an observation angle of $\beta=0°$ relative to the surface normal. In (b) and (c) results with attenuation are given for the observation angle $\beta=0°$ and 75°, respectively.

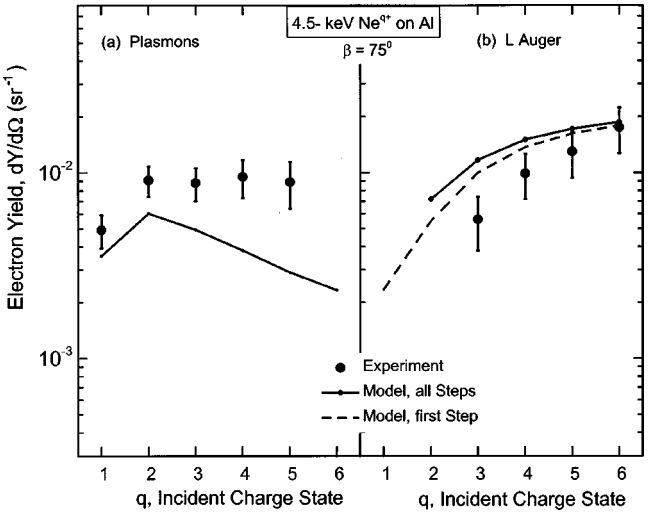

FIG. 7. Projectile charge state dependence of electron yields for 4.5-keV Ne^{q+} impact on Al. The results refer to electrons produced by plasmon decay (a) and Ne L-Auger transitions (b). The observation angle is $\beta=75°$ relative to the surface normal. The experimental results (points) are compared with model calculations using Eq. (4) for the first step (without above-surface emission) and the cascade formalism from Ref. [21] (solid curve) for all steps.

V. CHARGE-STATE DEPENDENCE

In addition to angular distributions, electron yields from plasmon decay were determined as a function of the charge state q of the incident Ne^{q+} ion. Figure 7(a) shows that the plasmon decay yield increases significantly (nearly by a factor of 2) as the charge state q changes from 1 to 2. For higher charge states, however, the plasmon decay yield remains constant within the experimental uncertainties. Figure 7(b) shows the corresponding electron yields for Ne L Auger emission, also obtained from the spectra in Fig. 1 (see the peaks labeled Ne). It should be pointed out that for decreasing projectile charge state it is difficult to separate the Ne L-shell Auger intensity from the continuous background. Therefore, in Fig. 7(b) we show Auger data for charge states $\geqslant 3$ only. In contrast to the plasmon decay data, the Ne L-shell Auger yield increases significantly with charge state. Considerations of the Ne L-shell Auger electrons are important, since they are produced by potential-energy transfer processes similar to those responsible for plasmon creation.

In Fig. 7 the charge-state dependence of the calculated yields are compared with the experimental data. Recall that the data refer to an electron emission angle of 75° relative to the surface normal. Figure 7(a) shows that the calculated electron yields from the plasmon decay are in reasonable agreement with experiment for the low charge states. In particular, the theoretical data show a similar increase as the experimental results when the charge state increases from $q=1$ to 2. However, when the charge states further increase, we observe raising discrepancies between theory and experiment. It is recalled that the plasmon-assisted capture process is favored for the charge states $q=1$ and 2 (Table II). These charge states are produced at the end of the filling sequence of the hollow atom so that the plasmon creation depth increases with increasing charge state. Hence, attenuation effects become increasingly important so that the decrease of the theoretical curve with increasing charge state may be understood.

In view of the discrepancies between the experimental and theoretical plasmon results, we may consider mechanisms different from the potential-energy transfer. Similar to the case of proton impact [13] plasmons may be excited in secondary interactions with high-energy electrons produced by the incident ions. The energies of electrons that are capable of exciting plasmons must exceed the threshold value of 18 eV. From Fig. 1 it is seen that the electron spectra exhibit long tails that reach into the range above the threshold. These electrons may partially be responsible for the observed production of plasmons. Continuous electrons with energies larger than 18 eV (33 eV inside the solid measured from the bottom of the band) are displayed in Fig. 8. It is seen that the yield of continuum electrons is rapidly increasing with the projectile charge state so that the continuous electrons are expected to gain importance at high charge states. It is seen that the yield of the electrons above 18 eV changes by a factor of ~ 20 as the charge state of the incident ions increases from $q=1-6$ (see Fig. 8). This is consistent with the finding in Fig. 7(a) that the deviation between the theoretical and experimental data for the plasmon creation increases with increasing projectile charge state.

Since the Ne L-shell Auger-electron production competes with plasmon creation, it is instructive to study also the emission yield of those electrons. In this case, above-surface effects [not modeled by Eq. (4)] may become important so that we used the extended formalism in which the corresponding differential equations had to be solved numerically [42]. It is found that the above-surface emission of Ne L-shell Auger electrons for an incident angle of 45° is relatively small and the survival factor f_o remains close to unity. The model calculations, which include also higher steps of the decay se-

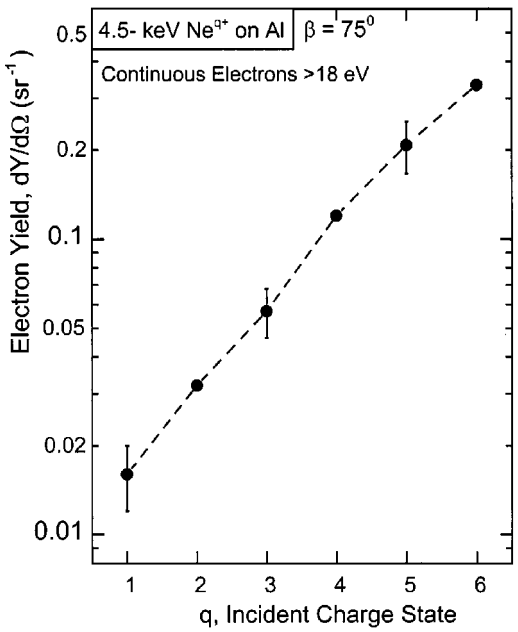

FIG. 8. Projectile charge state dependence of electron yields for 4.5-keV Ne^{q+} impact on Al. The results refer to electron yields obtained by integration of the continuous spectra above an energy of 18 eV. The observation angle is $\beta=75°$ relative to the surface normal.

quence, shown in Fig. 7(b). For comparison the results from Eq. (4), including only the first step of the decay sequence, are also displayed.

The theoretical results are found to be larger than the experimental data with increasing discrepancies for decreasing charge states. As mentioned before, the Ne *L*-shell Auger electrons are difficult to separate from the continuous background so that some Auger intensity may be lost. In particular, we note that the experimental results for the low charge states (e.g., $q=3$) represent the first step of the decay sequence only, since the higher steps produce Auger electrons shifted to lower energies which were not included in the integration procedure. The *L*-shell Auger electrons from the last step ($q=1$) occur in the region of the plasmon decay electrons. However, we would not expect that the Ne *L*-shell Auger electrons interfere with the plasmon yield determination. As described above, the plasmon yield results from the derivative of a *single* convolution over the conduction-band states with a sharp rise at the Fermi energy (Fig. 3). The Auger electrons originate from a *double* convolution, which smooths out the sharp structure at the Fermi edge, so that it can barely contribute to the electron yield derivative.

For higher charge states the experimental and theoretical results of the Ne *L*-shell Auger electrons tend to approach each other. A similar agreement has previously been found in a study of the Auger electrons using the high incident charge state $q=9$ [46]. We note that the previous results are consistent with the present charge state dependence of the yield of the Ne *L*-shell Auger electrons.

VI. CONCLUDING REMARKS

The present study is concerned with experimental and theoretical efforts to clarify mechanisms for plasmon creation by multiply charged neon moving slowly in Al. First of all, it is found that the plasmon production takes place well within the solid, since the angular distribution of the electron ejection closely follows a cosine distribution. This finding provides the basic condition for the search of the mechanisms for plasmon production.

Primary attention is devoted to capture processes which provide the potential energy necessary for the plasmon creation. The analysis of plasmons is accompanied by an analysis of projectile *L* Auger transitions. This is done because for neon projectiles the production of plasmon and *L*-shell Auger electrons is based on the same potential-energy effect. For small incident charge states, the experimental and theoretical results for the electron yield of the plasmon decay are found to be in reasonable agreement, whereas the theory overestimates Ne *L*-shell Auger-electron emission. The latter discrepancies are likely to be due to losses of Ne *L*-shell Auger electrons in the continuous background. On the other hand, at large incident charge states, increasing discrepancies observed between the model calculations and the experimental plasmon yields suggest mechanisms other than the potential-energy transfer producing plasmons. When analyzing the plasmon production, the contribution by secondary interactions with high-energy electrons should be considered.

Finally, let us look back at the methods implemented into the present cascade model. The attenuation of the electrons is taken into account in an approximate manner which is expected to introduce uncertainties into the present analysis. However, we do not expect that a more accurate treatment of the electron attenuation would change the essential conclusion of the present analysis. A problem may be involved in the value of the Ne *L*-shell filling rates Γ_L. For the low charge states $q=1$ and 2 of Ne^{q+} moving inside the solid we adopted filling rates which are consistent with previous work for helium [43]. Smaller rates for the *L*-shell filling have been evaluated in recent studies of hollow neon [47]. It should be noted, however, that the theoretical *L* Auger rates were determined for Auger transitions denoted *LCV*, where the excitation of the valence (*V*) electron is treated within the framework of linear-response theory. Due to the relatively high electron density of the *C* cloud [20] we expect an enhancement of the corresponding *LCC* Auger transition rate, where the valence-band electron is replaced by a *C* shell electron. In future work it would be useful to gain more theoretical information about the *LCC* transition rates.

Summarizing, we achieved progress in the understanding of plasmon production by slow impact of multicharged ions. Absolute values for the experimental electron yield from plasmon decay have been deduced. An analytic expression was derived to estimate the contribution of potential effects on the plasmon production. The comparison between theory and experiment suggests that for low incident charge states potential-energy effects are responsible for plasmon production, whereas at higher charge states secondary collisions with high-energy electron become important. However, the discussed mechanisms are not fully understood at present so that further work is needed to clarify various questions about plasmon creation by slow multicharged ions.

ACKNOWLEDGMENTS

We are grateful to Andres Arnau for his help in various collaborations and to Ricardo Díez Muiño for communication of his results prior to publication. We thank Itzam De Gortari and Jan-Hauke Bremer for their assistance in the experiments. R.B. thanks Carmina Monreal for stimulating discussions.

[1] J. Lindhard, K. Dan. Vidensk. Selsk. Mat. Fys. Medd. **28**, 8 (1954).
[2] D. Pines, *Elementary Excitations in Solids* (W.A. Benjamin Inc., New York, 1964).
[3] P. M. Echenique, F. Flores, and R. H. Ritchie, in *Solid State Physics: Advances in Research and Applications*, edited by H. Ehrenreich and D. Turnbull (Academic Press, New York, 1990), Vol. 43, p. 230.
[4] M.S. Chung and T.E. Everhart, Phys. Rev. B **15**, 4699 (1977).
[5] M. Rösler, Scanning Microsc. **8**, 3 (1994).
[6] T.E. Everhart, N. Saeki, R. Shimizu, and T. Koshikawa, J. Appl. Phys. **47**, 2941 (1976).
[7] C. Benazeth, N. Benazeth, and L. Viel, Surf. Sci. **78**, 625 (1978).
[8] D. Hasselkamp and A. Scharmann, Surf. Sci. **119**, L388 (1982).
[9] K.O. Groeneveld, R. Maier, and H. Rothard, Nuovo Cimento D **12**, 843 (1990).
[10] M. Rösler and W. Brauer, in *Particle Induced Electron Emission I*, edited by G. Höhler, Springer Tracts in Modern Physics Vol. 122 (Springer-Verlag, Berlin, 1991).
[11] R.A. Baragiola and C.A. Dukes, Phys. Rev. Lett. **76**, 2547 (1996).
[12] D. Niemann, M. Grether, M. Rösler, and N. Stolterfoht, Phys. Rev. Lett. **80**, 3328 (1998).
[13] S.M. Ritzau, R.A. Baragiola, and R.C. Monreal, Phys. Rev. B **59**, 15 506 (1999).
[14] B. van Sommeren, P. A. Zeijlmans van Emmichoven, I. F. Urazgil'din, and A. Niehaus, Phys. Rev. A **61**, 032902 (2000).
[15] P. Riccardi, P. Barone, A. Bonanno, A. Oliva, and R.A. Baragiola, Phys. Rev. Lett. **84**, 378 (2000).
[16] A.A. Almulhem and M. Girardeau, Surf. Sci. **210**, 138 (1989).
[17] R.C. Monreal, Surf. Sci. **388**, 231 (1997).
[18] F.A. Gutierrez, H. Jouin, S. Jequier, and M. Riquelme, Surf. Sci. **431**, 269 (1999).
[19] A. Arnau *et al.*, Surf. Sci. Rep. **27**, 113 (1997).
[20] N. Stolterfoht, D. Niemann, M. Grether, A. Spieler, A. Arnau, C. Lemell, F. Aumayr, and HP. Winter, Nucl. Instrum. Methods Phys. Res. B **124**, 303 (1997).
[21] N. Stolterfoht, A. Arnau, M. Grether, R. Köhrbrück, A. Spieler, R. Page, A. Saal, J. Thomaschewski, and J. Bleck-Neuhaus, Phys. Rev. A **52**, 445 (1995).
[22] A. Arnau, R. Köhrbrück, M. Grether, A. Spieler, and N. Stolterfoht, Phys. Rev. A **51**, R3399 (1995).
[23] R. Köhrbrück, M. Grether, A. Spieler, N. Stolterfoht, R. Page, A. Saal, and J. Bleck-Neuhaus, Phys. Rev. A **50**, 1429 (1994).
[24] M. Grether, A. Spieler, R. Köhrbrück, and N. Stolterfoht, Phys. Rev. A **52**, 426 (1995).
[25] D. Niemann, M. Rösler, M. Grether, and N. Stolterfoht, Nucl. Instrum. Methods Phys. Res. B **146**, 70 (1998).
[26] N. Stolterfoht, Z. Phys. **248**, 81 (1971).
[27] D. Niemann, M. Grether, A. Spieler, N. Stolterfoht, C. Lemell, F. Aumayr, and HP. Winter, Phys. Rev. A **56**, 4774 (1997).
[28] D. Hasselkamp and A. Scharmann, Vak.-Tech. **32**, 9 (1983).
[29] M. Delaunay, M. Fehringer, R. Geller, P. Varga, and HP. Winter, Europhys. Lett. **4**, 377 (1987).
[30] P.A. Zeijlmans van Emmichoven, C.C. Havener, and F.W. Meyer, Phys. Rev. A **43**, 1405 (1991).
[31] H. Kurz, F. Aumayr, C. Lemell, K. Töglhofer, and HP. Winter, Phys. Rev. A **48**, 2182 (1993).
[32] R.A. Baragiola, E. Alonso, and H. Raiti, Phys. Rev. A **25**, 1969 (1982).
[33] F. Xu *et al.*, Phys. Rev. A **50**, 4040 (1994).
[34] P. Sigmund and S. Tougaard, *Inelastic Particle-Surface Collisions*, edited by E. Taglauer and W. Heiland, Springer Series in Chemical Physics Vol. 17 (Springer, New York, 1981), p. 2.
[35] J. Burgdörfer, P. Lerner, and F.W. Meyer, Phys. Rev. A **44**, 5674 (1991).
[36] J. Ducrée, F. Casali, and U. Thumm, Phys. Rev. A **57**, 338 (1998).
[37] S. Winecki, C. Cocke, D. Fry, and M. Stöckli, Phys. Rev. A **53**, 4228 (1996).
[38] W. Huang, H. Lebius, R. Schuch, and N. Stolterfoht, Phys. Rev. A **56**, 3777 (1997).
[39] J. Burgdörfer, C. Reinhold, and F. Meyer, Nucl. Instrum. Methods Phys. Res. B **98**, 415 (1995).
[40] R. Page, A. Saal, J. Thomaschewski, L. Alberle, J. Bleck-Neuhaus, R. Köhrbrück, M. Grether, A. Spieler, and N. Stolterfoht., Phys. Rev. A **52**, 1344 (1995).
[41] H. Limburg, S. Schippers, I. Hughes, R. Hoekstra, R. Morgenstern, S. Hustedt, N. Hatke, and W. Heiland, Phys. Rev. A **51**, 3873 (1995).
[42] N. Stolterfoht, J.H. Bremer, and R. Díez Muiño, in *Multiply Charged Ions*, special issue of Int. J. Mass Spectrom. Ion Processes **192**, 425 (1999).
[43] M.A. Cazalilla, N. Lorente, R. Díez Muiño, J.-P. Gauyacq, D. Teillet-Billy, P.M. Echenique, Phys. Rev. B **58**, 13 991 (1998).
[44] R. Díez Muiño (unpublished). The calculations of the branching ratios are based on the formalism given in Ref. [47].
[45] E.C. Goldberg and J. Ferron, Surf. Sci. **172**, L523 (1986).
[46] M. Grether, A. Spieler, D. Niemann, and N. Stolterfoht, Phys. Rev. A **56**, 3794 (1997).
[47] R. Díez Muiño, N. Stolterfoht, A. Arnau, and P.M. Echenique, Phys. Rev. Lett. **76**, 4636 (1996).